Analysis and Experimental Study of the Flow Characteristics in a Micro-channel

Xiaorong Wang*, Jinxin Zhang, Genzhu Jiang, Guizhong Tian, Jingjing Shan

Institute of Mechanical Engineering
Jiang Su University of Science and Technology
Zhenjiang, China
E-mails: wrr31@qq.com, 920879172@qq.com, tbjcg@163.com, tianshuanger@126.com, 752525998@qq.com

Corresponding author

Received: October 22, 2014 **Accepted: December 1, 2014**

Published: December 19, 2014

Abstract: *To study the flow characteristics of low-speed fluid in a micro-channel, a model including the silk gland middle section, transition section, and forepart of a silkworm silk gland was established. The flow characteristics of silk solution therein were studied, and under the same average velocity, the flow characteristics of water were investigated for comparison with those of the silk solution. Results show that under the same average velocity, the axial velocity of the water was lower than that of the silk solution; the resistance coefficient change is the same, the resistance coefficient (both in the middle section and forepart) is constant, and in the conical channel, the resistance coefficient decreases linearly. At different average velocities, the variation of the water-related parameters was consistent; the conical channel differential pressure accounted for about 1.14% of the full differential pressure, and the straight channel pressure difference was 98.6%. With increasing outlet velocity, the shear layer of the silk solution gradually thinned, and the frictional pressure gradient decreased while the flow resistance also decreased. Later the flow characteristics of water and protein in the conical channel were studied and the changing relationship of the resistance coefficient and Reynolds number was analyzed. Finally, experimental research was undertaken on a micro-channel: the data were compared to simulated values, and the error was within 6%.*

Keywords: *Micro-flow, Micro-channel, Flow characteristic, Silk.*

Introduction

Although the increasing use of micro-channels has resulted in much research, discrepancies have been observed between different sets of published data [2, 5, 6, 8, 9, 14]. These discrepancies can be attributed to measurement uncertainties and scaling effects which include entrance effects, two-phase flow visualization, heat transfer effects, surface roughness, properties dependent on temperature, compressibility, and rarefaction.

Computational fluid dynamics (CFD) technology, applied to the study of micro-channel flow, has a number of applications. CFD simulations can be used to obtain detailed flow information including wall shear rate, pressure drops, and velocity. The strong dependence of flow patterns on vessel geometry and physiological conditions limits the use of idealized models, however, since interesting flow features may not be observed). Using CFD techniques and experimental comparisons, Rek and Zun [7] verified the independence of the grid in a micro-channel flow simulation.

Following CFD practice, a mesh independence study and a numerical model validation against published experimental data were both conducted. Analysis of the numerical simulation showed that channels with D = 100 μm can be characterized as micro-systems, while channels with D = 400 μm are mini-systems. Using the numerical simulation Lijo et al. [4] and others studied gas flow and heat transfer characteristics in micro-channels. Numerical simulations have been used to provide detailed flow characterization of micro-channel gas flows: the results obtained show that for choked flow conditions, high heat transfer is generated at both the entrance and the exit of the micro-channel. The exit effects, such as an increased strain rate, a high temperature gradient, and a thinning of the boundary layer generate a rapid increase in heat transfer at the exit of the micro-channel.

With the development of bionics, many papers focus on bionic micro-channel flow: Wu et al. [10] and others studied the flow of blood in a rectangular micro-channel. They studied two-dimensional blood flow characteristics in micro-channels using the open interface of a CFD routine. Finally, to understand this two-component flow system, and the effects of its different parameters, the equations were rendered dimensionless and a parametric study performed.

A numerical method is implemented for the analysis of unsteady blood flow through a branching capillary network by Davis and Pozrikidis [3]. The results of this continuum model are in agreement with the predictions of a discrete model where the motion of individual cells is followed from inlet to outlet.

Flow and heat transfer characteristics of swirling micro-channels of differing rectangular cross-sections have been experimentally investigated using 30% ethylene glycol solutions by Xi et al. [11]. Flow and heat transfer behaviours are compared with straight micro-channels: their results indicate that swirling micro-channels improve heat transfer performance by 50% on average.

For silk solution flow, the research has focused on electrostatic spinning fields [12, 13]. The understanding of the flow patterns in microfluidic devices is still relatively immature. To study the mechanisms at micro-scale, micro-structures and micro-features are devices used to obtain the flow characteristics of fluids in micro-channels. This represents a pressing problem for research into microfluidics, and will provide a theoretical basis for the design of new structures and devices. To study the flow characteristics of low speed fluids in a micro-channel, this research established a model of a silkworm silk gland middle section, transition section, and forepart to study the flow characteristics of silk solution therein. The data were compared with water's flow characteristics under the same average velocity. At the same time, we comparatively studied the characteristics of silk solution and water at different exit velocities. The changes in flow characteristics of different media along the axis of the channel were studied to find the relationship governing the changes in resistance characteristics at different velocities. Experimental research was done at different inlet pressures in a water flow in this micro-channel; we found the average speed, and compared it with simulated by way of verification.

Methods

Establishment of physical model

To obtain the physical model of a silkworm spinning channel, it was necessary to dissect a mature silkworm and acquire its spinning gland channel (Fig. 1). Using a microscope to obtain channel section sizes, the model of the spinning glands, including the mid-section and the back end of the gland, was established. The back end diameter of the chosen silkworm silk

gland was 0.12 mm, its length was 36 mm, mid-section diameter was 167 mm; the transition section of the cone tube measured 18.2 mm long. The silkworm's mid-part silk gland channel and posterior silk gland channel were used to establish the spinning channel model, due to the length-diameter ratio being larger (see the 10-fold expansion of the radial length in Fig. 2). The dimensions, as mapped, are in mm units and the entrance of the conical pipe was taken as the origin with the flow direction used as an x-axis, the radial direction as the r-axis, an x-coordinate at the entrance of the straight pipe of the silk gland mid-section of 5 to 10 mm, an x-coordinate at the taper of 18 mm, and an x-coordinate at the silk gland forepart's straight pipe of 54.2 mm.

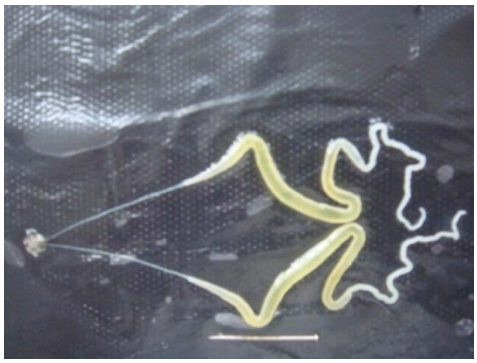

Fig. 1 Silkworm spinning channel

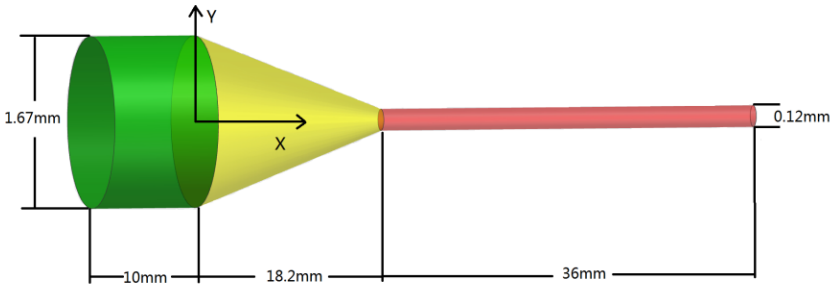

Fig. 2 Silkworm spinning channel model

Simplified model and boundary conditions

As the spinning channel is a rotating body, a two-dimensional axisymmetric model was used with its channel entrance, and outlet, pressures used, and a solid wall as a slip-condition adiabatic wall (see Fig. 3).

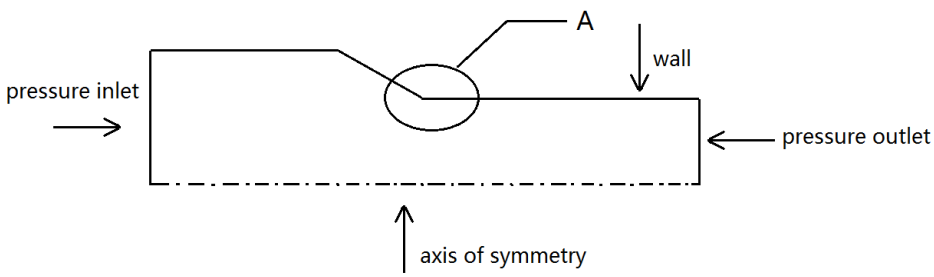

Fig. 3 Simplified model

Finite element simulations were performed using the COMSOL Non-Newtonian Fluid Flow solver. All simulations were isothermal. Mesh geometries were generated by COMSOL. The grid for orthogonal cases comprised 80 000 elements; a local grid amplification of a transition section is shown in Fig. 4.

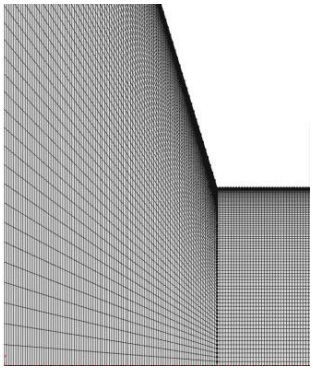

Fig. 4 Partial enlargement of the grid

Control equation

As $Kn < 0.1$, the control equation was continuous and the Navier-Stokes equations were

$$\frac{d\rho}{dt} + \rho \frac{\partial u_j}{\partial x_j} = 0 \tag{1}$$

$$\rho \frac{du_i}{dt} = \rho f_i - \frac{\partial}{\partial x_i}\left(p + \frac{2}{3}\mu \frac{\partial u_j}{\partial x_j} \right) + \frac{\partial}{\partial x_i}\left[\mu \left(\frac{\partial u_i}{\partial x_j} + \frac{\partial u_j}{\partial x_i} \right) \right] \tag{2}$$

Due to the flow being incompressible:

$$\frac{\partial u_j}{\partial x_j} = 0 \tag{3}$$

$$u_j \frac{\partial u_i}{\partial x_j} = -\frac{1}{\rho}\frac{\partial p}{\partial x_i} + \frac{1}{\rho}\frac{\partial}{\partial x_j}\left(\mu \frac{\partial u_i}{\partial x_j} \right) \tag{4}$$

Eq. (4) can be written as follows:

$$\frac{\partial}{\partial x_j}\left(\mu_j \varphi\right) = \frac{\partial}{\partial x_j}\left(\Gamma_\varphi \frac{\partial \varphi}{\partial x_j} \right) + S_\varphi \tag{5}$$

where φ is the general dependent variable and S_φ represents all the other phases that cannot be represented as convection or diffusion items.

For all simulations, values for conservation of mass and mesh convergence were checked to be within a tolerance of 5%. Mesh convergence was checked for conservation of mass at the inlet and outlet, as well as at nodal values for velocity along the gland length.

Non-Newtonian fluid viscosity

Bombyx mori silk solutions were obtained from Kojic. The Carreau-Yasuda model describes non-Newtonian viscosity by:

$$\eta(\dot{\gamma}) = \eta_0 \left[1 + (\dot{\gamma}\lambda)^a\right]^{(n-1)/a} \tag{6}$$

where η is the viscosity as a function of shear rate $\dot{\gamma}$, η_0 is the zero-shear viscosity, λ is a relaxation time for the fluid, a represents the rate of transition from zero-shear viscosity to shear-thinning behaviour, and n is the exponent characterising the shear-thinning regime. For *Bombyx mori* η_0 = 5200 Pa·s, λ = 0.57 s, a = 0.80, and n = 0.17 [1].

Model validation

To verify the independence of the grid, we meshed a straight pipe with a diameter of 0.12 mm and a length of 36 mm: the basic grid size matched the silkworm channel. Simulation of straight pipe flows has been done, the working medium used was water, the temperature was 300 K, the pressure difference across the system was 0.1 MPa, the outlet pressure was atmospheric pressure, and the outlet average velocity was approximately 1.25 m/s.

As *Re* = 150, flow in the pipe was laminar and using Poiseuille's formula to validate the findings, the error between exit velocity simulation values and theoretical values was less than 1.5%, as shown in Fig. 5.

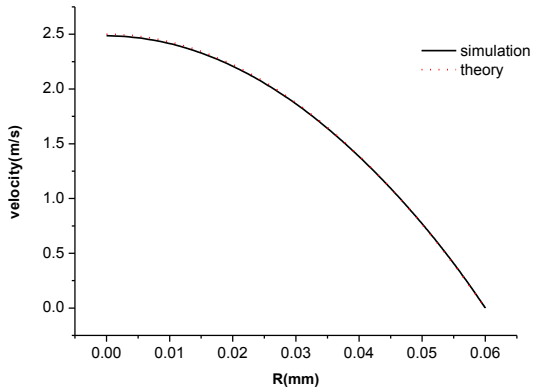

Fig. 5 Outlet radial velocity curve

Simulation results and analysis

Silk solution flow versus water flow in micro-channel

The literature shows that silkworm spinning rates are approximately 14 mm/s, from the flow simulation of a silk solution within silkworm mouthparts, the speed at the mouthpart entrance section is about 0.4 mm/s, so for a flow simulation of a silkworm channel, the working medium was a water/silk solution with repeated adjustment of the inlet pressure to ensure the outlet velocity remained at 0.1 mm/s: thus we compared the fluid characteristics of the two types of working fluids.

Fig. 6 shows the speed cloud of the water and silk solution in the silk gland, the pressure variation, and the velocity profile along the flow direction in the gland. Visibly, under the same average speed, the water and silk solution had different flow patterns: water is a Newtonian fluid, with a thick shear layer, a high-speed area which was narrow along its central axis, whereas the silk solution was a pseudo-plastic fluid, with a wide high speed zone near its central axis. Fig. 6c shows water and silk solution section profile average velocities along the flow direction in the silk gland. Visibly, in the straight pipe at the entrance (corresponding to the actual mid-section), the flow rate was low, water and silk solution velocity changes were consistent, and the silk solution velocity in the conical section was slightly higher than that of the water in the transition section. Both pressure change trends were consistent: the inlet pressure of the water was approximately 8 MPa, that of the silk solution reached 10 MPa.

Fig. 7 shows shear rate variations along the axial direction: from Fig. 7a and Fig. 7b, the area in which the shear rate was larger was concentrated at the forepart of the silk gland, and the water shear layer thickness was higher than that of the silk solution because the silk solution was a non-Newtonian fluid: in its high shear rate region, shear thinning dominated. Fig. 7c shows that the tendency of the shear rate along the silk gland channel was similar to that for the velocity. In the mid-section the shear rate remained practically unchanged, in the conical transition section the shear rate increased geometrically, and the silk gland's back end the shear rate remained steady with cross-sectional average shear rates respectively of: water, 2 1/s and silk solution, 3 1/s.

Fig. 7d shows the water as a Newtonian fluid: its radial shearing rate changed linearly, the wall shear rate was at a maximum, but the silk solution was non-Newtonian so its radial shearing rate increased slowly only to accelerate later over a cylindrical area such that $r < 0.0435$ mm. The silk solution shear rate was lower and bounded by $r > 0.0435$ mm. In the forepart of the silk gland channel, the water average shear rate was 2, the annular region in which the shear rate was higher than the average shear rate was $r > 0.023$ mm; the silk solution average shear rate was 3, and the area in which it was higher than the average shear rate was bounded by $r > 0.03$ mm. The shear layer of the silk solution was thinner than that of the water because of shear thinning in the silk solution: its viscosity decreased with increasing shear rate, so it had a thinner shear layer than its Newtonian fluid counterpart. This phenomenon made comparison of the two types of fluid possible at the same velocity: the silk solution fluid pressure drop was small, and it had a good liquidity.

Fig. 8 shows the radial velocity profile at different positions in the conical channel: 0 denotes the entrance, and 1 denotes its exit, and therefore 0.25 denotes a location a quarter of the way in from the entrance. The water velocity profile, at different sections, was parabolic, but because the silk solution underwent shear thinning, its cross-sectional velocity profile formed was blunted and was unlike the common parabolic velocity profile of Newtonian Poiseuille flow. So under the same average outlet velocity, the axial velocity of the water was lower than that of the silk solution, and its central high speed region was smaller. Therefore, the shear-thinning characteristics of the silk solution, also a feature of most other liquid crystalline polymers, greatly facilitated low-energy flow.

Fig. 9 shows the resistance coefficient along the whole silk gland channel; the resistance coefficient was constant through the mid-section and forepart straight pipe, but in the taper its value decreased linearly. The water resistance coefficient of the gland back end was approximately 5000, but the drag coefficient for the silk solution was approximately 6×10^{11}.

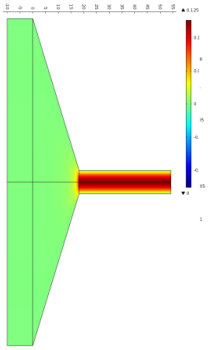

a) velocity cloud for water in a silk gland

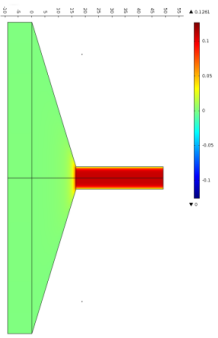

b) velocity cloud for silk solution in a silk gland

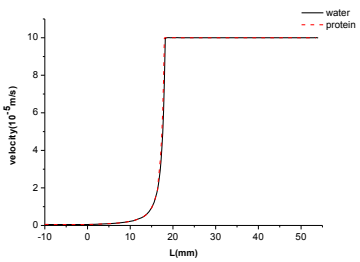

c) velocity profile

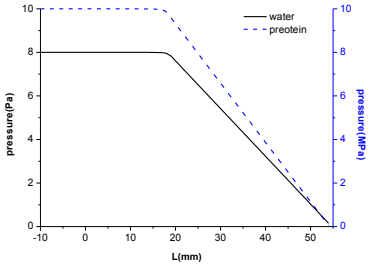

d) pressure variation

Fig. 6 Flow characteristics for different working media

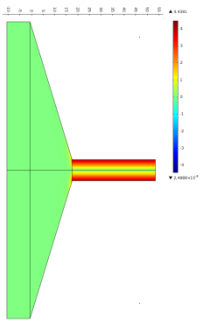

a) the shear rate cloud for water

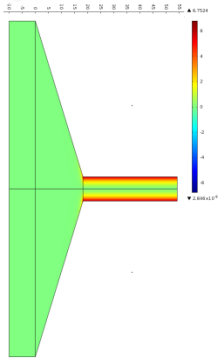

b) the shear rate cloud for a silk solution

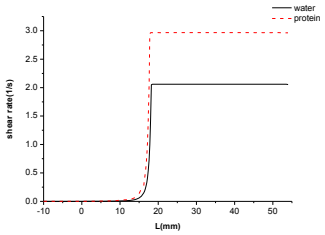

c) axial shear rate variation

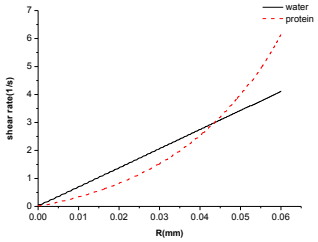

d) radial shear rate variation

Fig. 7 Shear rate variation

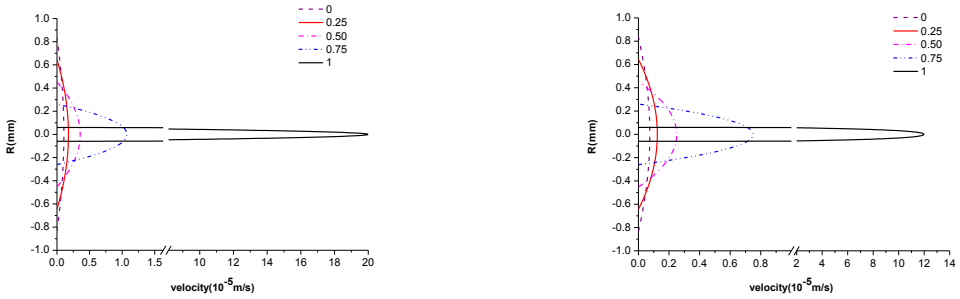

a) water b) silk solution

Fig. 8 Radial cross-sectional velocity profiles at various positions along the cone length

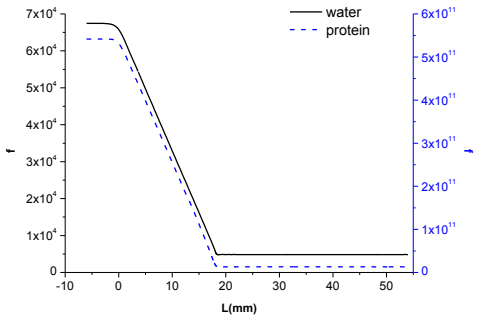

Fig. 9 Resistance coefficient versus axial position

Different outlet velocity flow characteristics of the water

To study the water pipe flow characteristics under different exit velocities, we simulated the flow of water under different average outlet speeds: 1 mm/s, 10 mm/s, and 100 mm/s respectively. Fig. 10 shows the radial cross-section velocity profiles at various positions along the cone lengths for a varying inlet velocity. The tapered transition section profile, along the axis, was a parabola and this shape, and its position, remained little changed, although the value doubled when the outlet velocity was increased. This shows that water flow in micro-channels was similar to macro-flow, therefore the macro-flow formula was still applicable. Fig. 11 shows flow field parameters and their variation along the flow path: for ease of comparison, these were normalised. For different exit velocities, the change in, and trend of, each parameter were consistent: when x < 10 mm the cross-section's average velocity along the flow direction changed slowly, from 0.005 at the entrance section to 0.02 in the conical channel (10 mm < x < 18.2 mm) where the velocity increased rapidly. The rate of increase was geometric with the decrease of the channel cross-section: at x = 10 mm, the velocity was 0.02, at the conical channel exit (x = 18.2 mm) the velocity rose to 1, and in the straight channel, it remained constant. In the conical channel, at x < 13 mm, the in-line pressure changed smoothly from 1 to 0.99986. At 10 mm < x < 18.2 mm, in the conical channel, the pressure reduced rapidly, from 0.99986 to 0.986. In the forepart of the silk gland channel, the pressure change was linear and its rate of change was independent of the flow in the channel. In the silk gland channel's forepart, the cross-sectional radial shear rate changed linearly, and its slope was constant for all modelled exit velocities. The shear layer thickness was also constant for different exit velocities. The pressure difference across the conical channel was only about 1.14% of that across the straight channel, and the straight channel pressure difference was 98.6% thereof.

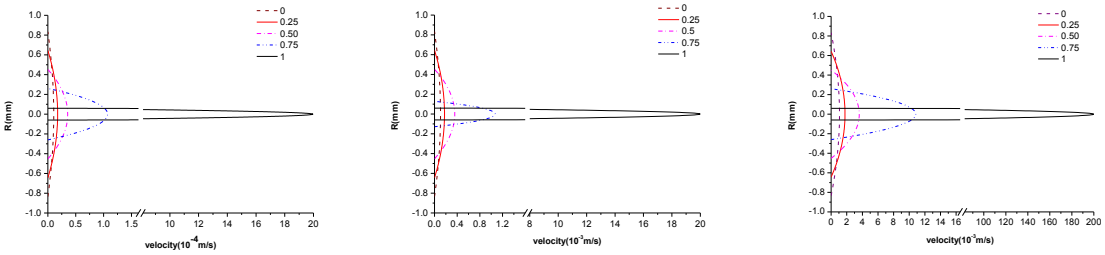

V_{out} = 1 mm/s V_{out} = 10 mm/s V_{out} = 100 mm/s

Fig. 10a Radial cross-section velocity profiles at various positions along the cone lengths for different outlet velocities

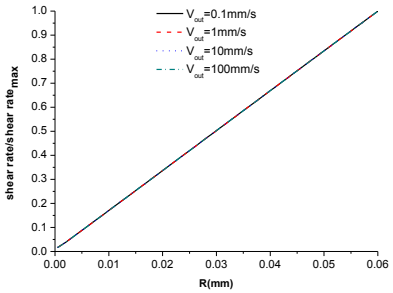

Fig. 10b Shear rate variations in the radial direction at the conical channel exit

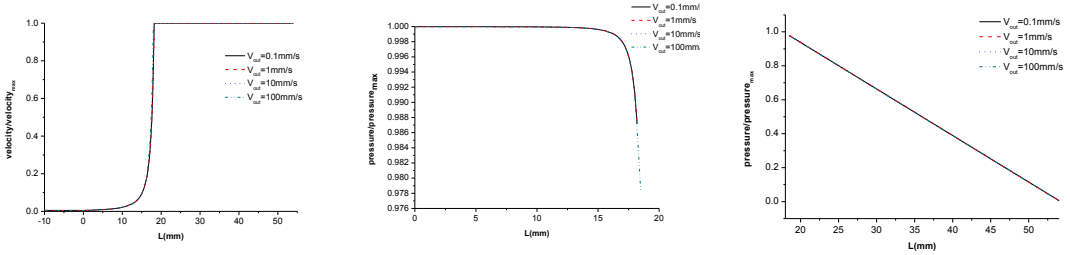

a) velocity versus position b) pressure versus position (in the conical channel) c) pressure versus position (in the silk gland forepart)

Fig. 11 Flow field parameter variations in the axial direction

Silk solution flow characteristics for different outlet velocities

Fig. 12 shows the silk solution's radial velocity variation along the each conical channel cross-section for different exit velocities: unlike water, the silk solution flow cross-section was blunted, and the greater the velocity, the slower its rate of change near the central flow axis. Fig. 12b shows that, with an increase in outlet velocity, the shear layer became thinner: because the shear rate increased near the axis, the shear thinning was more obvious, therefore, this governed the near-axis velocities, made them more consistent, and therefore the shear layer thinned. This shear thinning increased the liquidity of the silk solution.

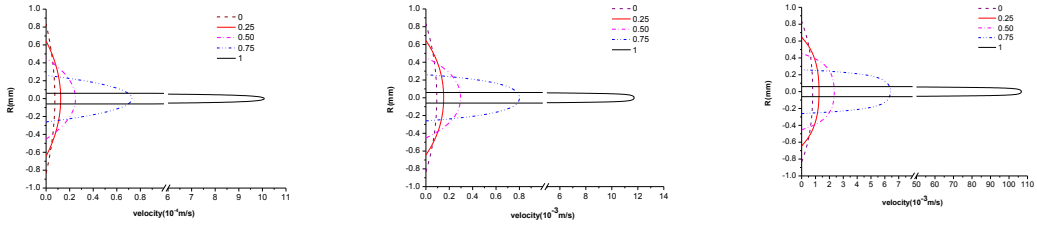

V_{out} = 1 mm/s V_{out} = 10 mm/s V_{out} = 100 mm/s

Fig. 12a Radial cross-section velocity profiles at various positions along the cone lengths for different outlet velocities

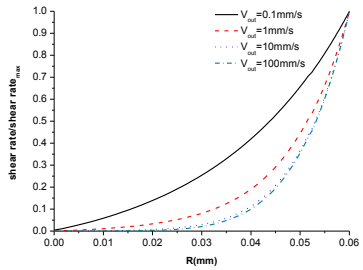

Fig. 12b Shear rate variation in the radial direction at the conical channel exit

Fig. 13 shows flow field parameter variations along the silk gland channels for different exit velocities: for ease of comparison these were normalised. Fig. 13a shows, for different exit velocities, that the silk gland channel had almost the same trend in its velocity. The trend in the velocity of the silk solution in the conical channel was also consistent: at -10 mm < x < 10 mm, the flow velocity changed slowly, for 10 mm < x < 18.2 mm (in the convergent conical channel) the velocity increased rapidly so that, at the conical channel exit, the velocity was 1. In the conical channel, the trend saw the pressure decrease slowly at first, but then do so more rapidly as the pressure gradient increased.

Fig. 13b shows that, with the increase of outlet velocity, the rate of drop in pressure along the axis increased: when the exit velocity was 0.1 mm/s, the channel section in which the pressure changed slowly spanned 0 mm < x < 16 mm and the pressure fell to 0.9998 at x = 16 mm. When the exit velocity was increased to 1 mm/s, this contracted to 0 mm < x < 10 mm, and when x = 16 mm, the pressure fell to 0.9992. With increased velocity, the channel section over which the pressure changed slowly contracted further: at 10 mm/s and 100 mm/s, the channel section over which the pressure changed slowly ws bounded by x = 3.6 mm and x = 1.8 mm respectively (with average pressures of 0.999 and 0.997, respectively). The increased flow velocity caused the pressure changes to be more gradual in the conical channel.

Fig. 13c shows that, for different exit velocities, the pressure in the silk gland forepart fell linearly, with increased flow velocity, the pressure gradient became slightly lower, and that increasing flow velocity could promote shear thinning in the silk solution thereby reducing its viscosity and reducing resistance to flow.

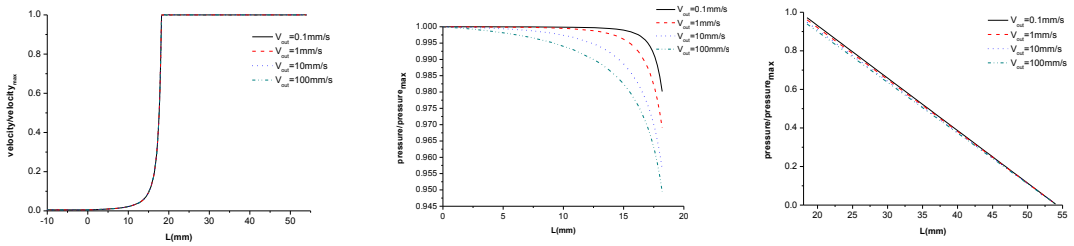

a) speed change curve along axis

b) pressure curves in conical channel

c) silk gland forepart pressure variation

Fig. 13 Parameter variation

In the first two thirds of the conical channel, along the flow direction, we took 10 cross-sections, and to the channel's back end we evenly placed a further 10 cross-sections in the final third thereof. At each cross-section we mapped the resistance coefficient and Reynolds number variations for both silk solution and water therein. These data are compared with macro-flow values, on a logarithmis axis in Fig. 14.

With the increase in Reynolds number, the drag coefficient of the water and the silk solution decreased: for equal Reynolds numbers, inside the micro-channel, at the end where the diameter was larger, the drag coefficient was also larger because the pressure drop was smooth before reaching the conical channel (see Fig. 11b and 13b). In the constant pressure section, the difference in resistance coefficient between the conical channel and straight channel was small, so the resistance coefficient versus Reynolds number curve for water matched the theoretical values for a Newtonian fluid. However, in the conical channel's back end, due to the pressure gradient being large, the resistance coefficient deviated from its theoretical value.

Throughout the channel, the drag coefficient (when using water) in the conical channel deviated from the theoretical values in the cylindrical straight channel by less than 4.3%. From the equivalent data for the silk solution, its, drag coefficient was much greater than that of water because the silk solution viscosity was also greater. When the silk solution velocity was small (i.e. at an exit velocity of 0.1 mm/s), the drag coefficient curve was quasi-linear, its slope matched the theory and the flow patterns were quasi-Newtonian (see Fig. 8b). With increased flow, i.e. at outlet velocities of 1 mm/s, 10 mm/s, and 100 mm/s, the slope of the curve decreased because the silk solution viscosity was rate dependent. Therefore, under the same flow rate and viscosity conditions as a Newtonian fluid, and when compared with the silk solution, the drag coefficient was lower and its liquidity enhanced.

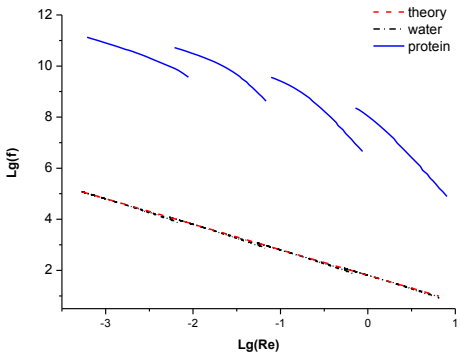

Fig. 14 Drag coefficient and Reynolds number along the conical transition section

Fig. 15 and 16 show that the water was indeed a typical Newtonian fluid: for an increase in velocity, the pressure change was linear and after taking logarithms, the Reynolds number had a linear relationship to the resistance coefficient. The discrepancy between drag coefficient and the theoretical value was less than 1.8%. The unit pressure drop in the silk solution-flow velocity curve was shown by the outermost convex curve, because the silk solution was a pseudo-plastic fluid. When its flow velocity was low, the unit pressure drop gradient became larger, as did the drag coefficient and after taking logarithms, the slope of the drag coefficient versus Reynolds number curve was quasi-Newtonian. Therefore with an increase in flow velocity, the unit pressure drop gradient decreased gradually and as indicated the silk solution viscosity decreased, the shear thinning phenomenon was significant, and the flow liquidity was enhanced.

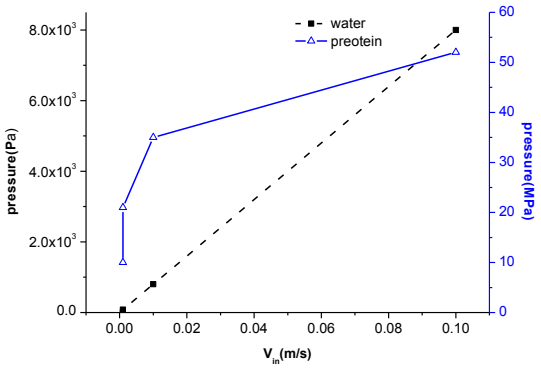

Fig. 15 Forepart flow velocity and unit pressure drop

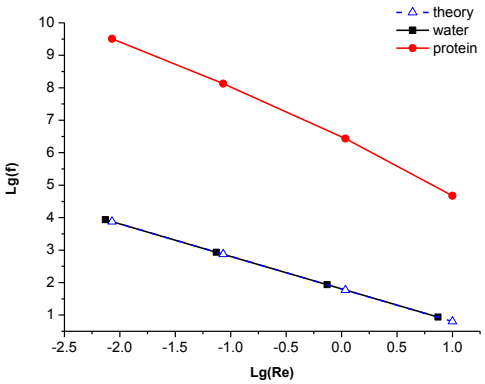

Fig. 16 Silk solution drag coefficient and Reynolds number variation

Experimental work

To verify whether or not the flow within a micro-channel can be solved using macro-flow theory, we conducted an experiment to test the relationship between average flow velocity and pipeline pressure difference in the silk gland's forepart. The apparatus comprised: a storage tank on a platform, by adjusting the liquid quality in the storage tank the inlet pressure could be adjusted; a digital display pressure sensor to read the average pressure in the channel inlet cross-section; an experimental pipeline; and rubber joint connectors with hard plastic joints to link the liquid storage tank to the system. The experimental channel was horizontal during testing, and the measuring cylinder was directly below the channel outlet. The flow rate was calculated using a timer, and the average flow velocity thus obtained.

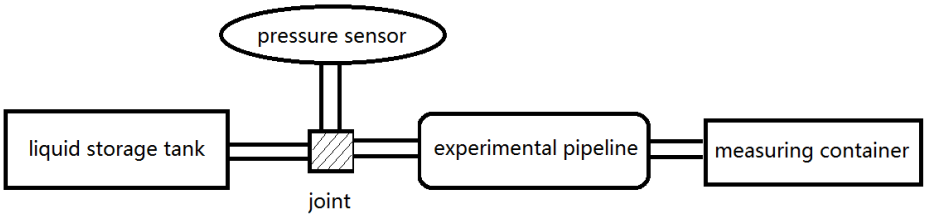

Fig. 16 Experimental apparatus (schematic)

The entrance pressures were 800 Pa and 8000 Pa. Three experiments were undertaken at each entrance pressure and the data averaged before being compared with the simulated results. Data are shown in Table 1 where P_{in} is the pressure at the entrance to the microchannel as

measured by a pressure gauge, Q is volume of flow in a 5 minute period, V_{avg} is the experimental average flow velocity, and V_{avgs} is the simulated average flow velocity. When the inlet pressure was 80 Pa, the experiment ran for 5 minutes; at 800 Pa and 8000 Pa, it ran for 1 minute.

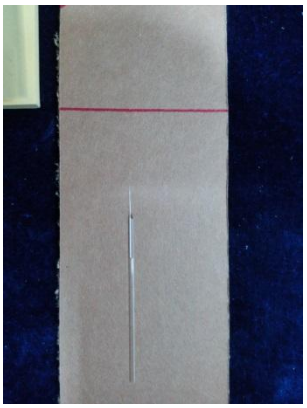

a) micro-channel

b) complete set-up

c) local amplification

Fig. 16 Experimental apparatus

Table 1. Experimental results versus simulated values

P_{in}, (Pa)	Q_1, (mL)	Q_2, (mL)	Q_3, (mL)	Q_{avg}, (mL)	V_{avg}, (mm/s)	V_{avgs}, (mm/s)	error
80	3.18	3.21	3.22	3.20	0.943	1	6.0%
800	6.44	6.41	6.45	6.43	9.48	10	5.4%
8000	65.4	65.3	64.9	65.2	96.1	100	4.1%

Compared with the simulated value, the experimental average flow velocity was smaller because during the experiment there were interfaces causing convex expansion losses, and the experimental equipment was poorly sealed. In general the discrepancy between simulated and experimental values was within 6% which validated the simulation.

Conclusions

Following conclusions can be summarized from this investigation:

1. At the same outlet velocity, the shear layer in the silk solution was thinner than that in water. The resistance coefficient changes in the two fluids were similar. In the straight channel (including the silk gland's forepart and mid-section) the resistance coefficient was constant, but in the conical channel, the resistance coefficient decreased linearly.
2. For different exit velocities, the changes in each water parameter were consistent along the x-axis. In the conical channel, the pressure difference was 1.14% of the total differential pressure and the straight channel pressure difference was 98.6%. With increasing outlet velocity, the shear layer in the silk solution gradually thinned, the pressure gradient decreased, and the resistance to flow decreased.
3. In the conical channel, the drag coefficient-Reynolds number curve for water was Newtonian. In the conical channel's back end, the resistance coefficient deviated from theoretical values but by no more than 4.3%. For the same Reynolds number, the drag coefficient of the silk solution was much greater than that of water: with increased flow velocity, the curve's slope gradually decreased, and viscosity of the silk solution decreased.

4. In the silk gland's forepart, after taking logarithms, the Reynolds number was linearly related to the flow resistance coefficient: the discrepancy between the drag coefficient and its theoretical value was less than 1.8%. The Reynolds number-drag coefficient curve for the silk solution was convex and as the drag coefficient increased, its slope decreased.
5. A micro-channel flow test was conducted. The relevant parameters for micro-channel flow were measured, and compared to simulated results: in general the discrepancy between simulated and experimental values was within 6% which validated the simulation.

Acknowledgements

The authors thank the National Natural Science Foundation of the Education Department, Jiangsu Province for contract 12KJB410001, the National Natural Science Foundation of China for contract 51005108, under which the present work was made possible.

References

1. Breslauer D. N., L. P. Lee, S. J. Muller (2009). Simulation of Flow in the Silk Gland, Biomacromolecules, 10, 49-57.
2. Cho S. C., Y. Wang (2014). Two-phase Flow Dynamics in a Micro Hydrophilic Channel: A Theoretical and Experimental Study, Int J Heat Mass Tran, 70, 340-352.
3. Davis J. M. C. Pozrikidis (2011). Numerical Simulation of Unsteady Blood Flow through Capillary Networks, B Math Biol, 73, 1857-1880.
4. Lijo V., H. D. Kim, T. Setoguchi (2012). Effects of Choking on Flow and Heat Transfer in Micro-channels, Int J Heat Mass Tran, 55, 701-709.
5. Liu W., C. Yang (2014). Two-phase Flow Visualization and Heat Transfer Performance of Convective Boiling in Micro Heat Exchangers, Exp Therm Fluid Sci, 57, 358-364.
6. Mansoor M. M., K. Wong, M. Siddique (2012). Numerical Investigation of Fluid Flow and Heat Transfer Under High Heat Flux using Rectangular Micro-channels, Int Commun Heat Mass, 39, 291-297.
7. Rek Z., I. Zun (2014). CFD Based Mini- vs. Micro-system Delineation in Elongated Bubble Flow Regime, Int J Multiphas Flow, 59, 73-83.
8. Sahin M., N. Balasubramanian, C. Misirli, H. E. Akata, Y. Can, K. Ozel (2012). On Properties at Interfaces of Friction Welded Near-nanostructured Al 5083 Alloys, The Int J of Adv Manufac Techn, 61, 935-943.
9. Wang Y., Z. Wang (2014). An Overview of Liquid-vapor Phase Change, Flow and Heat Transfer in Mini- and Micro-channels, Int J Therm Sci, 86, 227-245.
10. Wu W., N. Aubry, M. Massoudi, J. Kim, J. F. Antaki (2014). A Numerical Study of Blood Flow using Mixture Theory, Int J Eng Sci, 76, 56-72.
11. Xi Y., J. Yu, Y. Xie, H. Gao (2010). Single-phase Flow and Heat Transfer in Swirl Microchannels, Exp Therm Fluid Sci, 34, 1309-1315.
12. Zhang X., M. M. R. Khan, T. Yamamoto, M. Tsukada, H. Morikawa (2012). Fabrication of Silk Sericin Nanofibers from a Silk Sericin-hope Cocoon with Electrospinning Method, Int J Biol Macromol, 50, 337-347.
13. Zhou J., C. Cao, X. Ma (2009). A Novel Three-dimensional Tubular Scaffold Prepared from Silk Fibroin by Electrospinning, Int J Biol Macromol, 45, 504-510.
14. Zhu L., N. Kroodsma, J. Yeom, J. L. Haan, M. A. Shannon, D. D. Meng (2011). An On-demand Microfluidic Hydrogen Generator with Self-regulated Gas Generation and Self-circulated Reactant Exchange with a Rechargeable Reservoir, Microfluidics and Nanofluidics, 11, 569-578.

Xiaorong Wang, Ph.D.
E-mail: wrr31@qq.com

Xiaorong Wang is a lecturer and master tutor in the School of Mechanical and Engineering, Jiangsu University of Science and Technology, Zhenjiang, China. She is holder of a doctor degree. Her research interests are in the area of Computational Fluid Dynamics.

Jinxing Zhang
E-mail: 920879172@qq.com

Jinxing Zhang is a graduate student of the School of Mechanical and Engineering, Jiangsu University of Science and Technology, Zhenjiang, China. His research interests are in the field of Micro-flow Simulation.

Genzhu Jiang, M.Sc.
E-mail:tbjcg@163.com

Genzhu Jiang is a research assistant in the School of Mechanical and Engineering, Jiangsu University of Science and Technology, Zhenjiang, China. He is holder of a master degree. His research interests are in the field of Computational Fluid Dynamics.

Assoc. Prof. Guizhong Tian, Ph.D.
E-mail:tianshuanger@126.com

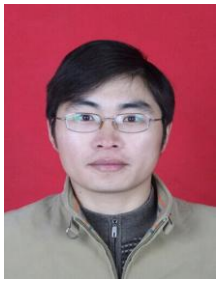

Guizhong Tian is an Associate Professor in the School of Mechanical and Engineering, Jiangsu University of Science and Technology, Zhenjiang, China. He is holder of a doctor degree and is a master tutor. His research interests are in the fields of Biomechanics and Biomechanical Engineering.

Jingjing Shan
E-mail: 752525998@qq.com

Jingjing Shan is a graduate student of the School of Mechanical and Engineering, Jiangsu University of Science and Technology, Zhenjiang, China. Her research interests are in the fields of Computational Fluid Dynamics and Micro Fluid Machinery.